RESEARCH ARTICLE

Macromolecular Bioscience
www.mbs-journal.de

HER2-Targeted, Degradable Core Cross-Linked Micelles for Specific and Dual pH-Sensitive DOX Release

*Nazende Nur Bayram, Gizem Tuğçe Ulu, Murat Topuzoğulları, Yusuf Baran, and Sevil Dinçer İşoğlu**

Here, a targeted, dual-pH responsive, and stable micelle nanocarrier is designed, which specifically selects an HER2 receptor on breast cancer cells. Intracellularly degradable and stabilized micelles are prepared by core cross-linking via reversible addition–fragmentation chain-transfer (RAFT) polymerization with an acid-sensitive cross-linker followed by the conjugation of maleimide–doxorubicin to the pyridyl disulfide-modified micelles. Multifunctional nanocarriers are obtained by coupling HER2-specific peptide. Formation of micelles, addition of peptide and doxorubicin (DOX) are confirmed structurally by spectroscopical techniques. Size and morphological characterization are performed by Zetasizer and transmission electron microscope (TEM). For the physicochemical verification of the synergistic acid-triggered degradation induced by acetal and hydrazone bond degradation, Infrared spectroscopy and particle size measurements are used. Drug release studies show that DOX release is accelerated at acidic pH. DOX-conjugated HER2-specific peptide-carrying nanocarriers significantly enhance cytotoxicity toward SKBR-3 cells. More importantly, no selectivity toward MCF-10A cells is observed compared to HER2(+) SKBR-3 cells. Formulations cause apoptosis depending on Bax and Caspase-3 and cell cycle arrest in G2 phase. This study shows a novel system for HER2-targeted therapy of breast cancer with a multifunctional nanocarrier, which has higher stability, dual pH-sensitivity, selectivity, and it can be an efficient way of targeted anticancer drug delivery.

1. Introduction

Breast cancer is the most common type of cancer among women. Today, using nanocarriers (NCs) in cancer treatment is advantageous due to their passive and active targeting ability.[1,2] Polymeric micelles that are formed by physical association of amphiphilic block copolymers are prone to disassemble with the dilution when introduced into the blood, causing premature drug release. In order to solve this problem and increase micelle's stability, cross-linking the core or shell parts of the micelle has emerged as an effective strategy.[3–6] Also, premature drug release from the micelles is still a problem in case drug is loaded by the incubation method, which is occurred by the weak physical interactions between the drug and the micelles. Therefore, many studies show that the chemical conjugation between the drug and the core cross-linked micelles (CCMs) can increase both stability and drug retention in the nanocarriers.[7,8] pH variation through the body and cell compartments is a prominent environmental factor to be used for targeting specific regions with micelles having stimuli-sensitive groups. Cross-linked micelles can be designed as "smart" so that they can be disrupted in the acidic pH of the cell while they are stable in the physiological environment, which can provide pH-sensitive drug release.[9] This can be achieved using degradable bonds or stimuli–responsive polymeric blocks in the structure of micelle NCs.[10] In cancer cell targeting, acid-sensitive bonds, which are acetal or hydrazone bonds, degrading at acidic pH values can be very convenient since these bonds can allow the dissociation of nanocarrier and releasing the drug molecules in lysosomes or endosomes of cancer cells.[10–12] It was shown that micelles cross-linked with acid-degradable agents exhibit much faster mode of action against cancer cells compared to the micelles cross-linked with nondegradable agents.

In order to reach multifunctionality with a nanocarrier, it can be conjugated with a targeting molecule so that it can selectively bind to target cells.[13] To do this, specific ligands that recognize cancer cells can be chemically incorporated into the nanocarrier, resulting in more selective drug release than conventional chemotherapy,[14,15] whereby, a higher amount of cytotoxic agent reaches the tumor site, and peripheral toxicity is minimized.

N. N. Bayram, S. Dinçer İşoğlu
Department of Bioengineering
Faculty of Life and Natural Sciences
Abdullah Gül University
Kayseri 38080, Turkey
E-mail: sevil.dincer@agu.edu.tr

G. T. Ulu, Y. Baran
Molecular Biology and Genetics
Faculty of Science
İzmir Institute of Technology
İzmir 35430, Turkey

M. Topuzoğulları
Department of Bioengineering
Faculty of Chemical and Metallurgical Engineering
Yildiz Technical University
İstanbul 34210, Turkey

The ORCID identification number(s) for the author(s) of this article can be found under https://doi.org/10.1002/mabi.202100375

DOI: 10.1002/mabi.202100375

Herein, we aimed to design a system comprising all required characteristics such as selectivity, stability, facilitated drug release behavior, and safety, with one nanocarrier. To achieve this, we prepared breast cancer targeted, core cross-linked micelles with double-moiety pH sensitivity (degradability) in which the drug is conjugated to the polymer with pH-sensitive hydrazone bonds and the micelle is core cross-linked with pH-sensitive acetal bonds. For the preparation of the micelles, we first synthesized the initial oligo-ethyleneglycol methyl ether methacrylate (OEGMA) block by reversible addition−fragmentation chain-transfer (RAFT) polymerization as the outer shell of micellar nanocarrier, and then it was copolymerized with diethylene glycol methyl ether methacrylate (DEGMA) and 4-vinylpyridine (4-VP) that will form the core of the micelle. To obtain CCMs, we used an acid-sensitive cross-linker (CL), which allows micelle formation during copolymerization at one pot. HER2-specific peptide (VSSTQDFP)[16,17] was conjugated to the shell of the micelle as the targeting moiety, while doxorubicin (DOX) was bound with acid-degradable acetal bonds to the micelle as the model drug against breast cancer cells. The cytotoxicity of the produced "smart" micellar NCs was investigated toward SKBR3 cells with the control of MCF-10A. Furthermore, HER2 peptide and DOX-conjugated micelles' apoptotic and cytostatic effects were evaluated on breast cancer cells. The "smart" polymeric micelle prepared in this study exhibits great potential as a multifunctional drug-conjugated carrier system with enhanced stability and dual pH sensitivity as HER2-targeted therapy for breast cancer.

2. Experimental Section

2.1. Materials

OEGMA (M_n = 500 g mol^{-1}), DEGMA, 4-VP, 2,2-dimethoxypropane (DMP), 2-hydroxyethyl methacrylate (HEMA), *p*-toluenesulfonic acid monohydrate (p-TSA·H_2O), tris(2-carboxyethyl)phosphine (TCEP) hydrochloride, doxorubicin hydrochloride, 2,2-dithiodipyridine (DTDP), ethanolamine (ETA), 4-cyano-4-(thiobenzoylthio)pentanoic acid (CTA), azobisisobutyronitrile (AIBN), 4,4-azobis(4-cyanovaleric acid) (ACVA), triethylamine, *Nε*-maleimidocaproic acid hydrazide (EMCH), trifluoroacetic acid (TFA) salt, *N*-(3-dimethylaminopropyl)-*N′*-ethylcarbodiimide hydrochloride (EDC), *N*,*N*-diisopropyethylamine (DIPEA), and 1-hydroxybenzotriazole hydrate (HOBT) were purchased from Aldrich and used as received. Synthetic peptide (VSSTQDFP) was purchased from CASLO Laboratory ApS. Pierce Quantitative Fluorometric Peptide Assay was purchased from Thermo Scientific. All other chemicals used were of analytical grade. SKBR-3 (HER2 positive human mammary gland/breast adenocarcinoma) cell lines were purchased from ATCC (HTB-30). MCF-10A (HER2 negative human mammary gland/breast non-tumorigenic) cell line (ATCC CRL-10317) was kindly provided by Prof. Ayşe Elif Erson Bensan, Middle East Technical University. 2,3-bis-(2-methoxy-4-nitro-5-sulfophenyl)-2H-tetrazolium-5-carboxanilide (XTT) cell proliferation assay kit (Roche) and paraformaldehyde (PFA) powder were purchased from Sigma–Aldrich. 4′,6-diamidino-2-phenylindole dihydrochloride (DAPI) powder dye was obtained from Invitrogen. Annexin V/propidium iodide (PI) dual staining apoptosis assay kit and propidium iodide were provided by Biolegend. TGX Stain-Free FastCast acrylamide kit (10%), Trans-Blot Turbo RTA Transfer Kit-PVDF, Clarity Western ECL Substrate, and Trans-Blot Turbo Transfer System were obtained from Bio-Rad. ab32124-anti-Bcl-2 antibody (E17), ab32503-anti-Bax antibody (E63), ab184787-anti-Caspase-3 antibody, ab9485-anti-glyceraldehyde-3-phosphate dehydrogenase (anti-GAPDH) antibody (Loading control), ab205718 goat antirabbit immunoglobulin G (HRP) were provided from Abcam. RNase-A, the pancreas was obtained from Biomatik.

2.2. Methods

2.2.1. Synthesis of CCMs

First of all, macro chain transfer agent (macroCTA,Poly(OEGMA)) and cross-linker were synthesized according to the Topuzoğulları et al., Bhuchar et al., and Boyer et al. studies, respectively, and the details is given in the Supporting Information.[18–21] The following step was the preparation of core cross-linked micelles by RAFT polymerization. To synthesize the micelle, macroCTA was dissolved in 5 mL of water, and then, varying amounts of 4-VP (1.0–0.25 mmol) and DEGMA (1.0–0.3 mmol) together with CL (1–10% mmol) were added. The reaction was performed overnight at 60 °C using ACVA as the initiator (**Scheme 1**). The formation of the cross-linked micelles was also confirmed by the turbidity formed in the solution. After the overnight reaction, the solution was dialyzed against water to remove unreacted substance. The chemical structures of purified copolymer micelles were characterized by Fourier transform infrared (FTIR) and proton nuclear magnetic resonance (^{1}H-NMR) spectroscopies, while the size and size distribution of the samples were determined by dynamic light scattering (DLS) spectroscopy. Selected samples, which were CCM2 and CCM5, were analyzed by a transmission electron microscope (TEM) to examine sizes and morphologies.

2.2.2. Preparation of Drug-Conjugated and Targeted NCs

Pyridyl Disulfide Modification of CCMs: Pyridyl disulfide (PDS) modification of the CCM through its core region for conjugation of the drug molecule was carried out according to the procedure in literature.[22] Briefly, 500 mg of CCM2 and dithiodipyridine (70 mg, 3.2×10^{-4} mol) were dissolved in dimethylformamide (DMF ,2 mL). The vial was sealed by rubber septum and purged with N_2 for 10 min. Ethanolamine (36.37 mg, 6.0×10^{-4} mol) was dissolved in DMF (1 mL) and 150 µL of this solution was added to the vial under N_2. The mixture was stirred at room temperature for 4 h. The yellow-colored mixture was precipitated from cold diethyl ether and dried under vacuum. The product was dissolved in water and then dialyzed against water/methanol (50:50) and only water, respectively. The product given in **Scheme 2**A was lyophilized and examined by a ^{1}H-NMR spectroscopy.

Maleimide-Modified DOX Synthesis: To synthesize maleimide-functionalized DOX (MALDOX), first, DOX·HCl (30.2 mg, 0.052 mmol) was neutralized with triethylamine (15.8 mg, 0.156 mmol). The mixture was dialyzed against water to remove redundant unreacted triethylamine and then the DOX solution

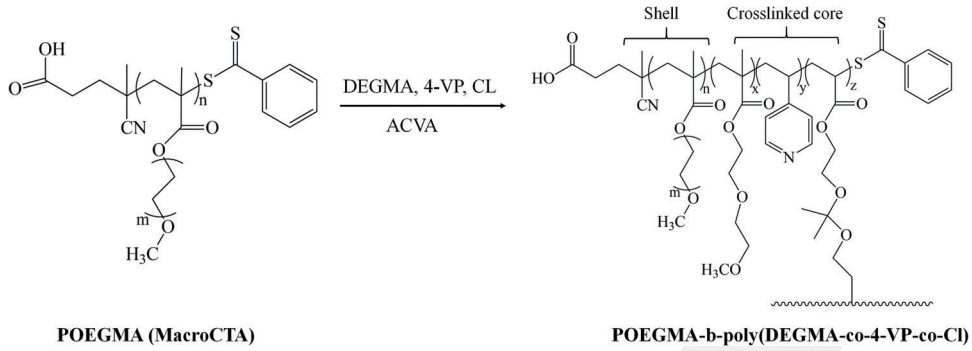

Scheme 1. Synthesis of core cross-linked micelles by RAFT polymerization using macroCTA.

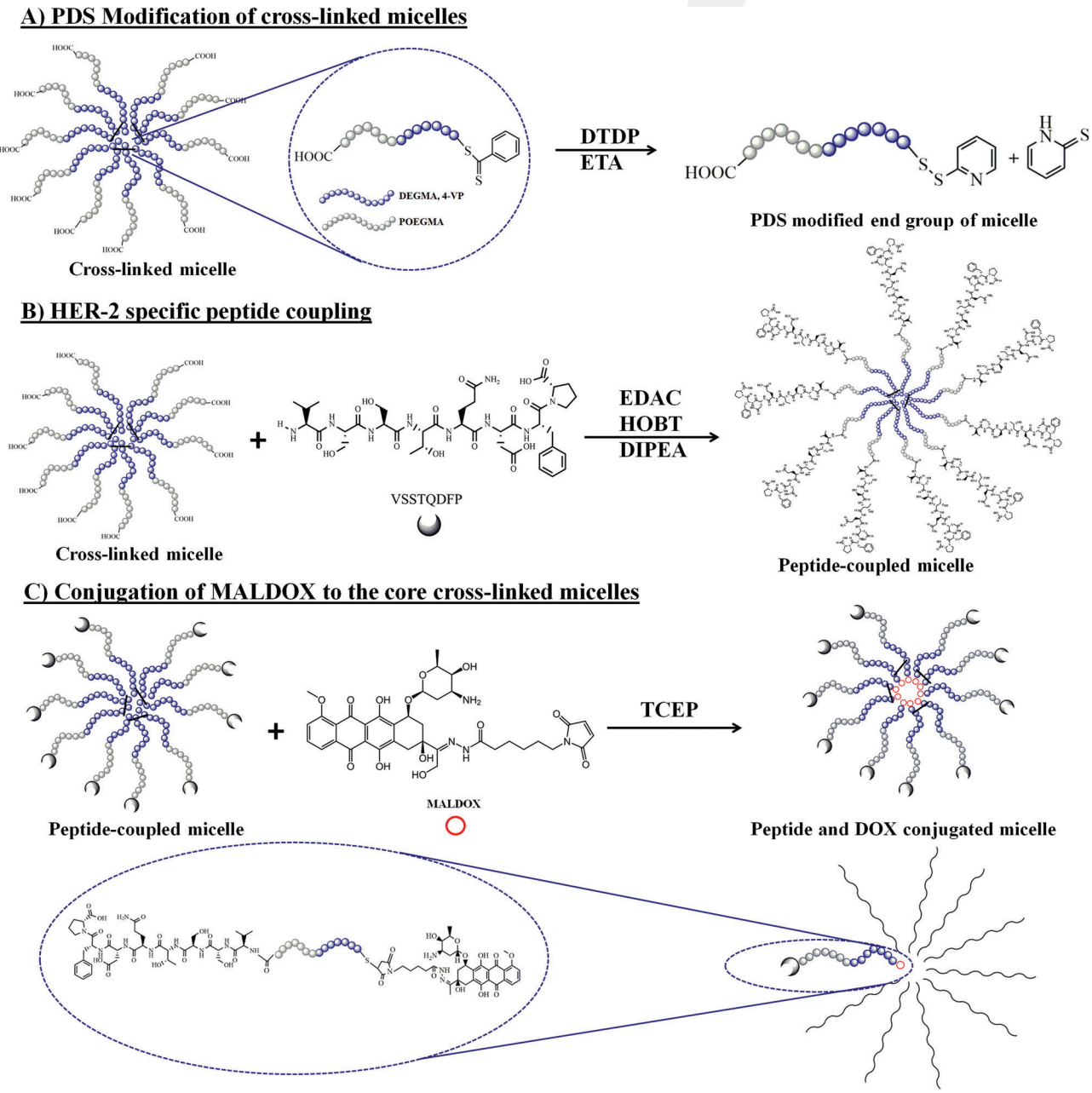

Scheme 2. Drug and peptide conjugation to the core cross-linked micelles.

was lyophilized. Following this, DOX (12 mg, 2.07×10^{-5} mol) and EMCH (14 mg, 4.1×10^{-5} mol) were dissolved in dry methanol (6 mL), and a few drops of TFA were added. The mixture was stirred overnight in the dark, and then, methanol was removed using a rotary evaporator. The remaining mixture was precipitated using dry ethyl acetate. The final product, MALDOX, was stored under a vacuum. The pure sample was analyzed by ^{1}H-NMR and high-resolution matrix assisted laser desorption/ionisation time-of-flight mass spectrometry (MALDI-TOF MS).[8]

HER2-Specific Peptide Conjugation: For peptide incorporation to the shell part of the CCM2, first, 100 mg of CCM2 was dissolved in 3 mL of dimethyl sulfoxide (DMSO)/DMF (3:1) mixture, stirred at 60 °C overnight, and the sample was taken from the oil bath and cooled to 25 °C. EDC (3.07 mg), HOBT (2.23 mg), DIPEA (4.18 µL), and peptide (14.08 mg, VSSTQDFP) were added to this mixture and stirred at 60 °C for 2 days. The mixture was dialyzed against the water with a 3500 Da molecular weight cut-off (MWCO) membrane.[14] The product was lyophilized and analyzed by ^{1}H-NMR spectroscopy (Scheme 2B).

Conjugation of MALDOX to CCMs: In this step, CCMs carrying the PDS group were conjugated to MALDOX (depicted in Scheme 2) by using TCEP, as seen in Scheme 2C. Briefly, 100 mg of micelle and MALDOX (3.75 mg, 5×10^{-6} mol) were dissolved in 4 mL dry methanol and then TCEP (1.44 mg, 5×10^{-6} mol) was dissolved in dry methanol (2 mL) and added dropwise to the reaction medium. Subsequently, the mixture was stirred overnight in the dark and then dialyzed against dry methanol for 2 days, and the resulted product was precipitated from diethyl ether three times. The final product was stored under vacuum for analysis with ^{1}H NMR spectroscopy.[8]

2.2.3. Characterization

NMR spectra of the samples were acquired by Bruker 400 (EUTAUM) or Bruker Ultrashield 300 MHz liquid NMR spectrometers using related deuterated solvents. Size, size distributions, and zeta potential of the samples were obtained using Malvern Zetasizer NanoZS DLS and electrophoretic light scattering (ELS) spectrometry at 25 °C using a refractive index value of 1.5. Samples were dissolved in water for size measurement, water, and phosphate-buffered saline (PBS) for charge measurement. High contrast TEM (CTEM, 120 kV, METU Central Laboratory) was used to examine the size and morphology of the samples. The concentration of the samples dissolved in water was prepared between 0.1% and 1% (w/v), and then examined after drying by dropping 3–5 µL on a carbon-coated grid. Molecular weight and molecular weight distributions of the polymers were determined by a Viscotek TDA302 gel permeation chromatography (GPC) system with Shim-Pack GPC804 column using tetrahydrofuran (THF) as the mobile phase. The flow rate was 0.8 mL min^{-1} and polystyrene (PS) (M_w = 99 000 g mol^{-1}, polydispersity index (PDI) = 1.05, dn/dc = 0.165) was used as the single standard to calibrate the detectors. Mass spectra of the samples were acquired from an Ultraflextreme MALDI-TOF MS (Bruker Daltonics, USA) equipped with a nitrogen UV–laser operating at 355 nm. Spectra were recorded in reflection positive mode with an average of 5000 shots. Dihydroxybenzoic acid (DHB) was used as the MALDI matrix. Matrix and sample solutions were mixed to obtain a W_{sample}/W_{matrix} ratio of 1:5. About 1 µL of matrix/sample mixture was deposited on the sample plate, dried at room temperature, and analyzed.

2.2.4. Release Study

1 mL of doxorubicin-conjugated micelle solution was placed in dialysis membrane tubes (Fisherbrand Regenerated Cellulose Dialysis Tubing, 3500 Da MWCO). The whole tube was placed into citrate buffer (pH 4.5) or PBS (pH 7.4) and shaken (70 rpm) at 37 °C.

At certain time intervals, 1 mL of buffer solution was withdrawn, and the fresh buffer was added. The release of the active substance was determined by measuring the absorption (at 496 nm[23]) of the DOX molecule in withdrawn buffers, and the following formula was used to acquire the cumulative release plots[23]

$$\mathrm{CR}\,(\%) = [(100 \times ((V_m \times C_{\mathrm{DOX}(n)}) + (1\mathrm{mL} \times \Sigma C_{\mathrm{DOX}(n-1)}))]/W_0 \quad (1)$$

According to this, V_m is the emission media volume; W_0 (mg) is the amount of drug loaded; $C_{\mathrm{DOX}\,(n)}$ is the amount of DOX (mg mL^{-1}) in the sample taken from the release medium; $C_{\mathrm{DOX}\,(n-1)}$: $(n-1)$ is the amount of DOX in the sample taken from the media.[24]

2.2.5. Degradation Study of CCMs

To evaluate the acid-triggered degradation of the micelles, the micelle solutions were incubated at pH 4.5 up to 24 h and samples were taken from the mixture at different time intervals and analyzed by FTIR and DLS. GPC was also used in order to follow degradation in different acid-exposure time.

2.2.6. Cell Culture Studies

Preparation of Cell Lines: SKBR-3 (HER2 positive breast cancer cells) and MCF-10A (HER2 negative nontumorigenic breast cells) were used to determine the effect of DOX-conjugated NCs. SKBR-3 and MCF-10A cell lines were used to compare the targeting efficiency of synthesized NCs, separately. SKBR-3 cells were grown in Dulbecco's Modified Eagle Medium (DMEM) high glucose with 1% L-glutamine, 10% Fetal Bovine Serum (FBS) , and 1% Pen-Strep. Also, MCF-10A cells were grown in DMEM nutrient mix F12 (1:1) with 1% L-glutamine, 10% horse serum, 1% Pen-Strep, 20 ng mL^{-1} Epidermal growth factor (EGF) , 0.5 µg mL^{-1} hydrocortisone, 10 µg mL^{-1} insulin, and 100 ng mL^{-1} choleratoxin. Note that, in all cytotoxicity analyses, experiments were conducted in triplicate in at least three independent experiments, and statistical analysis was done using paired t-test, and $p < 0.05$:*; $p < 0.01$:**; and $p < 0.001$:*** were considered significant.

2.2.7. Determination of Cytotoxic Effects of NCs on Cells

XTT solution was prepared with XTT labeling reagent:electron-coupling reagent (Roche) using a 50:1 dilution ratio. Different concentrations of NCs were applied to the cells. After 48 or 72 h, 50 µL of prepared XTT solution was added into each well. Next, a 96-well plate was incubated in an incubator with 5% CO_2 at 37 °C for 6 h. Finally, the formation of orange formazan dye was detected at 450 nm with spectrophotometry (Thermo Electron Corporation Multiskan Spectrum).

2.2.8. Intracellular Uptake of NCs on Cells

After incubation of NCs on cells, 2 mL per well, 3.7% paraformaldehyde was added and incubated for 20 min. After incubation, PFA on cells was discharged and washed with 2 mL per well 1× PBS twice. Then, 1:500 DAPI in 2 mL 1× PBS was added in each well and incubated for 30 min. Ten different images were taken for each well at Alexa-555 for 210.5 ms with Olympus-IX83 fluorescence microscopy. Then, image analysis based on fluorescence intensity density was accomplished by using ImageJ software. Also, three different images were taken at DOX, and DAPI fluorescence and co-localization values were determined by the Fiji program. Note that SKBR-3 cells grown in 6-well plates (5×10^5 cells per well) and MCF-10 cells grown in 6-well plates (3×10^5 cells per well) were treated with half-maximal inhibitory (IC_{50}) doses of DOX-NCs-HER2 and DOX-NCs at 48 h. Experiments were done in triplicate—at least three independent experiments—and statistical analysis was done using unpaired *t*-test, $p < 0.05$:*; $p < 0.01$:**; and $p < 0.001$:*** were considered significant for ten different images sections. The error bars represent the standard deviations.

2.2.9. Determination of Apoptotic Effects of NCs on Cells

Apoptotic effects on SKBR-3 cells were determined by Annexin V/PI double staining and western blotting. After incubation of nanocarriers on cells, the cells were collected and centrifuged. The cell pellet was then dissolved with 200 µL per well Annexin binding buffer. About 2 µL of fluorescein isothiocyanate (FITC) labeling of recombinant annexin V or/and 2 µL of propidium iodide (PI) were added. The tubes were incubated at room temperature for 15 min. Finally, apoptotic or necrotic cells were detected with flow cytometry (BD FACS Canto).

Bcl-2, Bax, and Caspase-3 protein expression levels were determined by western Blotting. After incubation of NCs on cells, the cells were collected and centrifuged. After centrifugation, the supernatant was removed, and the pellet was dissolved with Tris buffer, which contains 10×10^{-3} M Tris-HCl, 1×10^{-3} M Ethylenediaminetetraacetic acid (EDTA) , and 0.1% Triton-X. They were centrifuged at 14 000 rpm for 20 min. After the cell lysed, the protein concentration was determined by using SMARTTM BCA protein assay kit.

About 30 µg of cell-lysed protein was loaded in each well and separated on 10% sodium dodecyl sulfate-polyacrylamide (SDS-PAGE) gel. After running protein samples, proteins were transferred onto the polyvinylidene difluoride (PVDF) membrane using a Trans-Blot SD Semi-Dry transfer cell (Bio-Rad) according to the manufacturer's recommendations. 1:1000 Bcl-2 (Abcam-ab32124-anti-Bcl-2 antibody (E17)), 1:1000 Bax (Abcam-ab32503-anti-Bax antibody (E63)), 1:2000 Caspase-3 (Abcam-ab184787-anti-Caspase-3 antibody) were used as positive control. Proteins were incubated overnight at 4 °C. After incubation, 1:3000 immunoglobulin G (IgG) (Abcam-ab205718 goat antirabbit IgG (HRP)) was used as a secondary antibody. Next, 1:2500 GAPDH (Abcam-ab9485-anti-GAPDH antibody) was used for loading control. Bcl-2, Bax, Caspase-3, and GAPDH bands were detected using enhanced chemiluminescence reagents supplied by Bio-Rad in an image processor (Fusion SL Vilber Lourmat). Prestained protein, SHARPMASSTM VI Protein MW, marker was used for the loading marker. Protein bands were quantified by densitometric analysis using ImageJ software. Resulting Bcl-2, Bax, and Caspase-3 values were adjusted for normalization by GAPDH protein. Experiments for apoptotic analysis were done in triplicate—at least three independent experiments.

2.2.10. Determination of Cytostatic Effects of NCs on Cells by Cell Cycle Analysis

Cytostatic effects on SKBR-3 cells were determined by PI staining. After incubation of nanocarriers on cells, the cells were collected and centrifuged. After centrifugation, the supernatant was removed, and the pellet was dissolved with 1 mL of cold PBS and placed in the icebox for 15 min. Next, 4 mL of ethanol was added into the tubes and kept in the freezer at −20 °C overnight. Next, the cells were centrifuged at 800 rpm for 5 min. After centrifugation, the supernatant was removed, and the pellet was dissolved in 1 mL of cold PBS. Again, the cells were centrifuged at 800 rpm for 5 min. After centrifugation, the supernatant was removed, and the pellet was dissolved with 1 mL of PBS-(0.1%) Triton X 100. Next, 100 µL RNase-A was added and incubated at 37 °C for 30 min. After incubation, 100 µL PI was added and incubated at room temperature for 10 min. Finally, the different phases of the cell cycle were detected with flow cytometry. Experiments for cell cycle analysis were done in triplicate—at least three independent experiments.

3. Result and Discussion

3.1. Synthesis of CCMs

The core cross-linked micelles were synthesized by copolymerization of 4-VP and DEGMA through the chain end of POEGMA macroCTA in different ratios of components with the presence of cross-linker (yield = 77%). Here, micelle formation and copolymerization were occurred simultaneously, due to the cross-linking reaction and RAFT polymerization. Cross-linked micelles via RAFT polymerization in the presence of a cross-linker have already been reported in literature.[4,5,8,19,25] The obtained copolymer micelles were examined structurally by FTIR and ^{1}H-NMR spectroscopies. In the FTIR spectrum (Figure S2, Supporting Information), the band at 1720, 2870, and 1100–1245 cm^{-1} assigned to the groups of C=O, $-CH_2-$ ($-CH_3$), and C–O–C, respectively.

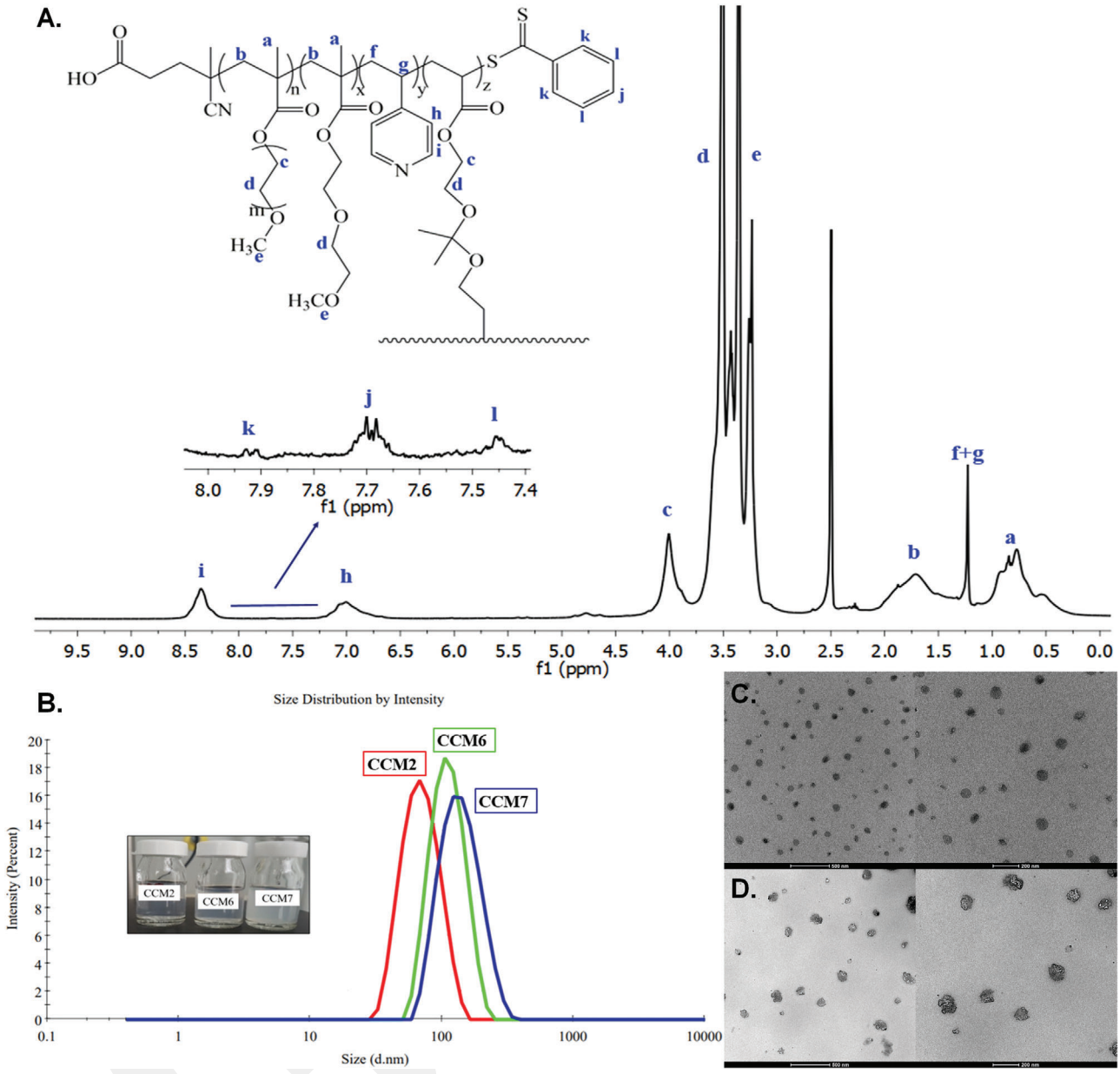

Figure 1. A) ^{1}H NMR spectrum of CCM2 in DMSO-d_6. B) Size measurements of selected micelles (CCM2, CCM6, and CCM7). C,D) TEM images of C) CCM2 and D) CCM5 at different magnifications.

The peak intensity obtained at 1720 cm^{-1} increased due to the addition of the cross-linker and DEGMA, while the peaks around 2900 and 3000 cm^{-1} were obtained due to the $-CH_2-$ and $-CH_3$ groups in other units. In addition, an increase in the C–O–C peak at 1245 cm^{-1} was caused by the cross-linker. The addition of 4-VP to the structure was determined from the C=N stretch peak obtained around 1600 cm^{-1}.

The ^{1}H-NMR spectrum, given in **Figure 1**A, reveals the successful synthesis of cross-linked micelles in which 4-VP protons are clearly observed at 7.0 and 8.5 ppm. Similar to the macroCTA's NMR spectrum (Figure S1, Supporting Information), the peaks related to ring protons of RAFT agent were obtained between 7.5–8 ppm as tiny peaks. Then, micelles dissolved in water were analyzed with DLS spectrometry in terms of size and size distribution at 25 °C. The results given in **Table 1** clearly show that micelles having diameters between 10 and 144 nm were obtained successfully with low PDI values. The increase in the internal structure of micelles with 4-VP and DEGMA ratios (0.25–1 and 0.25–0.75 mmol, respectively) resulted in a noticeable increase in micelle size. Once we increase the amount of cross-linker, chance of cross-linking reaction between the components and polymerization reaction increases. It also increases the number of polymer chains in the core, which connected to another polymer chain, and finally a cross-linked core. Depending on the amount of cross-linker, we obtain a denser core structure and it eventually forms bigger micelles. The size

Table 1. Hydrodynamic diameters and PDI values of cross-linked micelles synthesized by using different amounts of DEGMA, 4-VP, and cross-linker (CL).

Sample	DEGMA [mmol]	4-VP [mmol]	CL [%]	Hydrodynamic diameter [nm]	PDI
CCM1	0.25	0.25	5	10	0.161
CCM2	0.5	0.25	5	70	0.126
CCM3	0.75	0.25	5	83	0.161
CCM4	0.75	0.25	1	78	0.212
CCM5	0.75	0.25	10	116	0.175
CCM6	0.75	0.5	5	115	0.078
CCM7	0.75	1	5	144	0.123

difference of micelles is also noticeable from the appearance of the aqueous solutions. In Figure 1B, the size distributions of the micelles with hydrodynamic diameters of 70, 115, and 144 nm are given. In addition, TEM images of CCM2 and CCM5 are shown in Figure 1C,D. The diameter of the micelle determined by TEM was compatible with those measured by DLS spectrometry. In the next steps of the study, CCM2 was used for the drug binding and peptide conjugation owing to the low PDI value and hydrodynamic diameter between 10 and 100 nm for the optimum enhanced permeability and retention (EPR) effect.[26]

3.2. Preparation of Targeted and Drug-Conjugated Nanocarriers

3.2.1. PDS Modification of Micelles and MAL–DOX Synthesis

In order to chemically bind the drug, first, the ω-end of the polymer chain was converted to the PDS group (Scheme 2A) (yield = 75%). In the study of Boyer et al., the chemical shift of the ring protons attributed to RAFT agent (at 7.4–7.5–7.8 ppm) shifted to 7.1–7.6–8.4 ppm, following the conversion to PDS.[22] In our study, **Figure 2** shows that these peaks shifted to around 7.3–7.6–8.4, which confirms PDS modification. Also, the color of the micelles solution turned to yellow, which is also confirms PDS modification.

In order to conjugate the drug to the micelles via the PDS group, DOX·HCl was converted to DOX–maleimide (DOX–MAL) in which maleimide and DOX are linked with an acid-degradable hydrazone bond. In the studies that used hydrazone bonds between DOX and MAL, the released DOX after degradation of hydrazone bond in acidic environment maintains its activity.[27,28] The maleimide modification in DOX was confirmed by structural analysis with ^{1}H-NMR spectroscopy. According to **Figure 3**, the expected peaks of maleimide and hydrazone were shown at 7.0 and 9.4 ppm, respectively. Furthermore, DOX–MAL ($C_{37}H_{42}N_4O_{13}$) was analyzed by a high-resolution MALDI-TOF MS, and the molecular ion signal was observed as 809.24 (m/z) (Figure S3, Supporting Information). This ion is the result of the addition of Na^+ and K^+ ions by the separation of acidic hydrogen

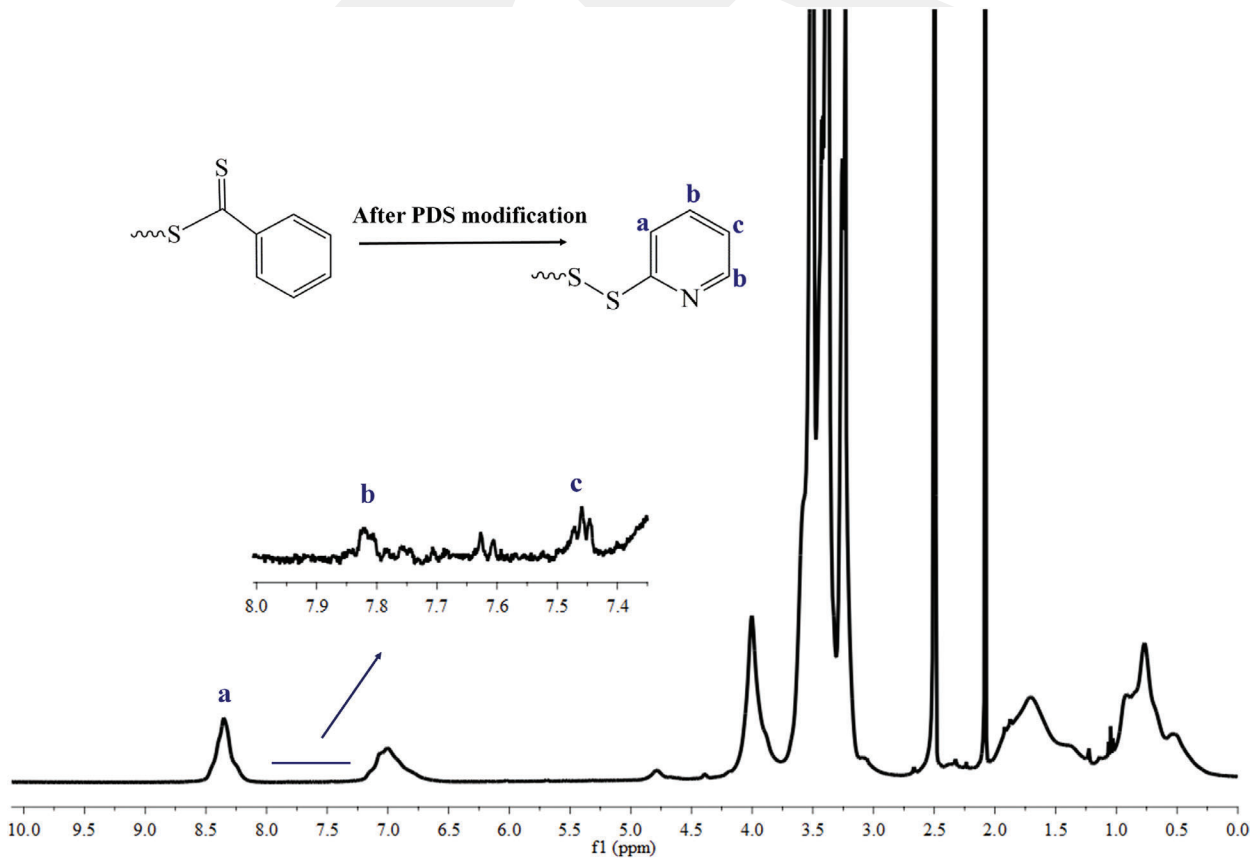

Figure 2. ^{1}H-NMR spectrum of the CCM obtained by conversion of ω-end to PDS in DMSO-d_6.

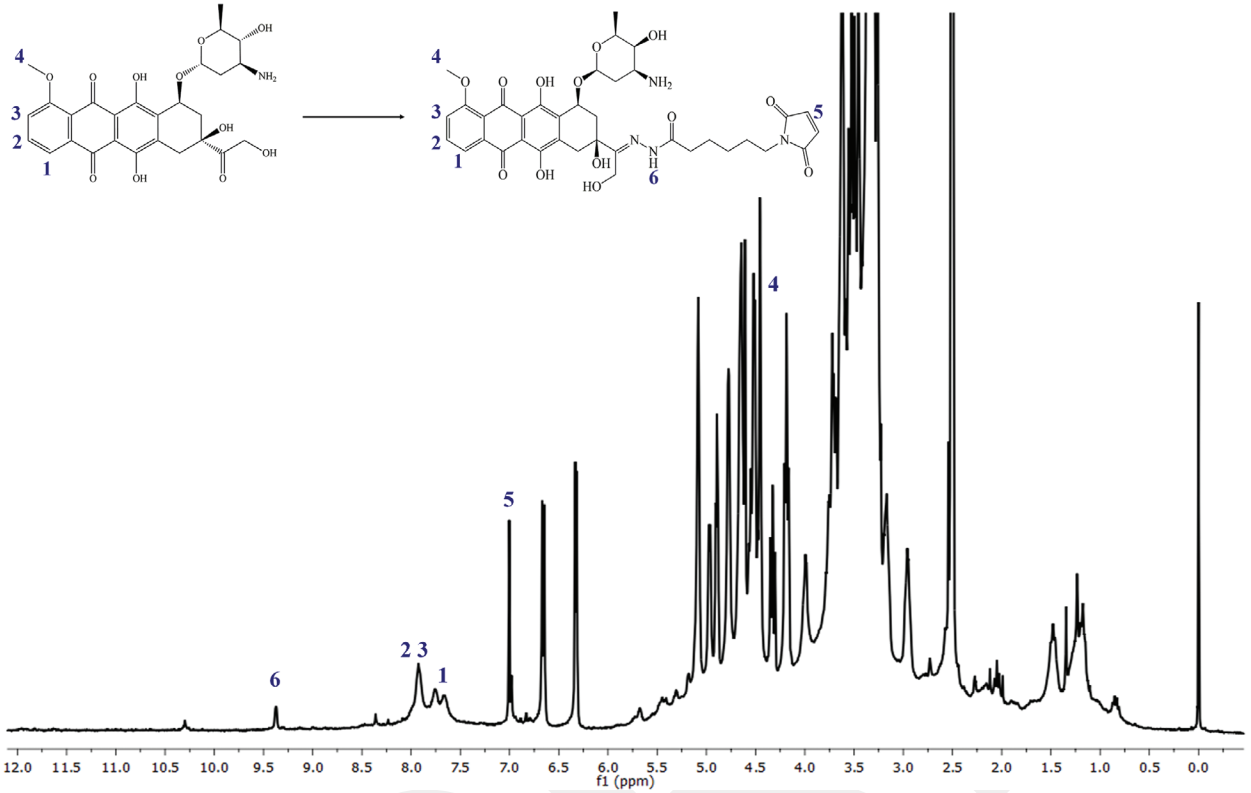

Figure 3. ^{1}H-NMR spectrum of MALDOX in DMSO-d_6.

atoms in the molecular structure. The mass values below 700 m/z are the disintegration signals formed by the cleavage of some groups from the MAL–DOX molecule and they coincide with the theoretical cleavage values.[8]

3.2.2. Binding of Targeting Ligand (HER2-Specific Peptide) and DOX Conjugation to the Micelles

The HER2 targeting peptide of VSSTQDFP was activated by NHS via the amino group, and then covalently bound to the carboxyl end group from the RAFT agent on the micelle of CCM2 in the presence of carbodiimide (EDC) (yield = 79%).[14] **Figure 4**A–D shows ^{1}H-NMR spectra of micelles with A) PDS modification, B) DOX-conjugated micelles, C) peptide-conjugated micelles, and D) peptide- and DOX-conjugated micelles, respectively. In Figure 4A–C, the peaks of the peptide and micelles were compared, and the amide bond of the peptide could not be differentiated due to existing amide bonds in the cross-linked micelles, but the peaks associated with the peptide were observed to increase the intensity, unlike Figure 4A. Furthermore, peaks of the benzene ring in phenylalanine were observed at 7–7.5 ppm, and the methyl peak of threonine and the proton of the aspartic acid–proline hydroxyl groups were shown at 1.2 and 10.2 ppm, respectively. Size measurement was also performed, and the size of the peptide-bound micelles increased from 70 to 90 nm (Figure S4, Supporting Information). According to ^{1}H-NMR spectra and size measurements, the peptide was successfully conjugated to micelles. In addition to this, peptide conjugation was also confirmed by Pierce Quantitative Fluorometric Peptide Assay (Thermo Scientific, USA). The peptide-conjugated CCM2 sample was dissolved in water at a concentration of 1 mg mL^{-1}, and fluorescence was measured using Ex/Em at 390 nm/475 nm. According to the calibration graph given in Figure S5 (Supporting Information), the measured fluorescence corresponding peptide amount was determined as 7.30 ± 1.56 µg mL^{-1}.

Following the peptide coupling to micelles, the prepared MALDOX was conjugated to micelles and MALDOX-bound peptide coupled micelles were characterized by ^{1}H-NMR spectroscopy. Figure 4B–D shows the ^{1}H-NMR spectra of MALDOX-conjugated micelles and MALDOX–peptide-conjugated micelles, respectively. In Figure 4B–D, the hydrazone group of MALDOX was clearly observed at around 9.5 ppm, which confirmed the conjugation of MALDOX to the micelle and peptide-coupled micelles. Also, the methyl peak of DOX was shown at 4–5 ppm. In the study of Jia et al., the peak of maleimide proton (observed with EMCH-modified DOX, Figure 3) at 6.97 ppm was not present in the spectrum of DOX–micelle conjugate, revealing the reaction between the free thiol groups of the micelle and the maleimide group of DOX.[8] However, in our study, the absence of these peaks was not determined because a signal for the micelles at 7 ppm was present. As another confirmation for drug binding to micelle, the absorbance spectra of the DOX-conjugated samples were examined by a UV-spectrophotometer (Figure S6, Supporting Information).[29–32] Accordingly, when the spectra of micelle and drug-bound micelle were compared, the absorbance value at 502 nm of the drug was observed as 0.316, while it was 0.027 for micelle, which indicates that the drug was bound to the

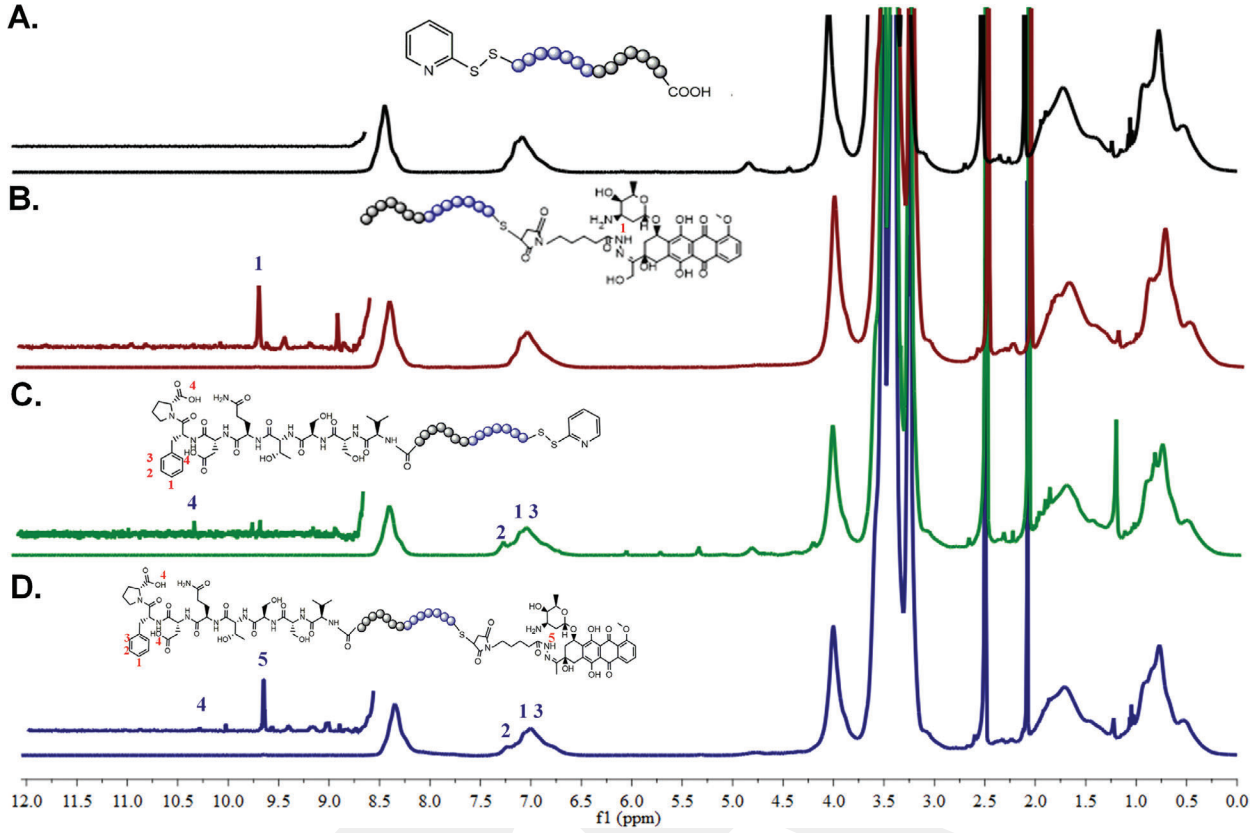

Figure 4. ^{1}H-NMR spectra of A) micelles with PDS modification, B) DOX-conjugated micelles, C) peptide-conjugated micelles, and D) peptide and DOX-conjugated micelles in DMSO-d_6.

micelle. Here, DOX quantity of CCM2 and peptide-conjugated CCM2 were obtained as 2.4 ± 0.07% (w/w) and 1.6 ± 0.08% (w/w) with 63 ± 1.8% and 42 ± 2.1% conjugation efficiency, respectively. The relatively low rate of doxorubicin conjugation in the peptide-linked micelle compared to the peptide-unconjugated micelles may be caused by the inability of MALDOX to reach the core part due to the steric hindrance created by the peptides conjugated in the shell. Also, the size of DOX-conjugated CCM2 and DOX and peptide-conjugated CCM2 were 99 nm and 116 nm, respectively (Figure S7, Supporting Information). In addition, the zeta potential of the micelles is an important feature, as it affects the blood residence time and cellular uptake of the micelles. The zeta potentials of the DOX-conjugated CCM2 and DOX and peptide-conjugated CCM2 (in water) are −18.23 ± 0.51 and −16.90 ± 0.36, respectively. Also, these values in PBS are −6.24 ± 0.47 and −6.45 ± 0.34 for the DOX-conjugated CCM2 and DOX and peptide-conjugated CCM2, respectively.

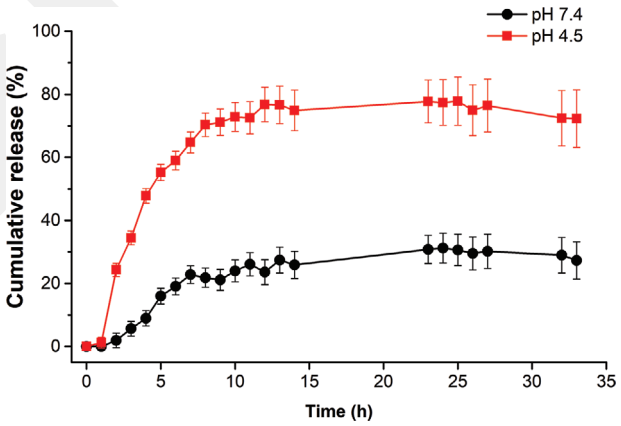

Figure 5. Cumulative release of DOX from cross-linked micelles at pH 4.5 (■) and 7.4 (●).

3.3. Drug Release Studies

Due to the acidic character of intracellular endocytic vesicles and tumor environment, we conjugated DOX to the CCMs by acid-cleavable hydrazone linkage to obtain a polymeric smart system that can be stimulated by acidic pH through these sites for the drug release. In addition to the hydrazone linkage, acid-degradable acetal-based cross-links in the micellar core will also contribute to the micelle disintegration and drug release. In this work, the release study was performed at pH 7.4 which is a characteristic for blood circulation, and at pH 4.5 for mimicking subcellular acidic organelles whose pH value is 4.5–5.5.[33,34] **Figure 5** shows the cumulative release of DOX at pH 4.5 and 7.4 from the DOX-conjugated core cross-linked micelles as a function of time. As seen, 78% of DOX was released from the micelle at pH 4.5 by pH-based cleavage of acetal and hydrazone bonds, while only 31% of DOX was released at pH 7.4 in 24 h, which reveals that

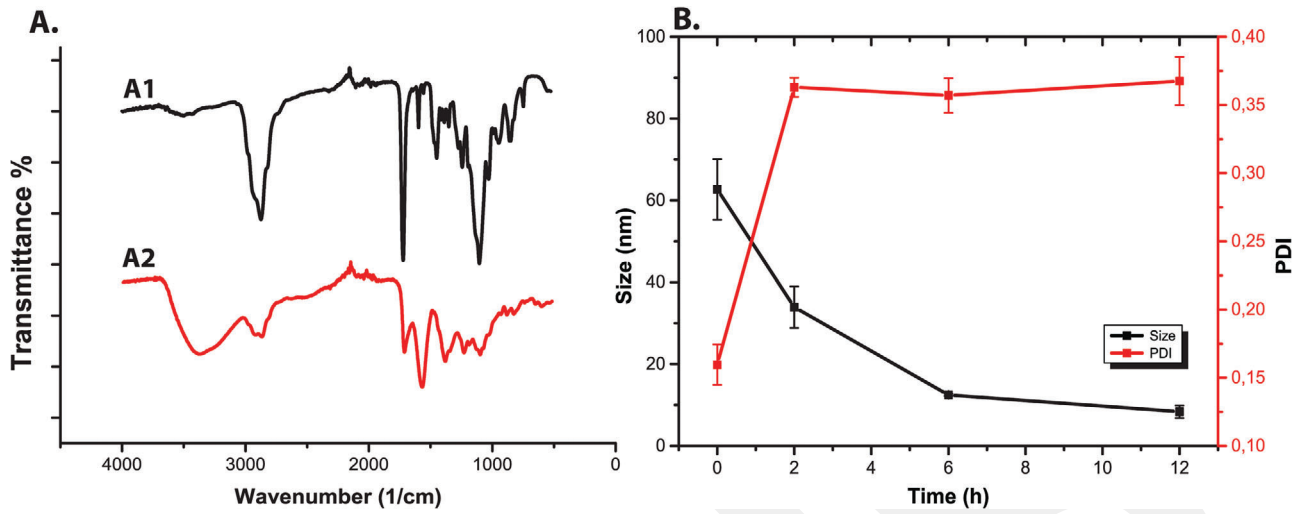

Figure 6. A) FTIR spectra for A1) before A2) after micelle degradation. B) Size and size distribution of micelles in PBS depending on acid exposure time.

core cross-linked micelles exhibit a pH-dependent drug release profile.

In the release profile at pH 4.5, a burst release was observed in the first 5 h, and more than 55% of the drug is released. Within the first 5 h, there was about 15% DOX release at pH 7.4, which might be attributed to unconjugated DOX physically entrapped inside the particles as also reported in a similar study by Wong et al.[35] Note that, we applied dialysis against ethanol at least for 2 days after the conjugation process, which was supposed to be sufficient to remove the physically bound MALDOX according to the literature.[8] However, presence of other components in the micelle structure might cause additional physical interaction with DOX by possible $\pi-\pi$ stacking between DOX and pyridine aromatic rings. It is important to note that micelles do not release a fraction of DOX molecules (22%) at pH 4.5, which can be explained by the dynamic nature of hydrazone bonds and interactions of doxorubicin with the degraded hydrophobic segments of the copolymer, as also explained in similar studies.[36,37] According to the Qi et al. study, they synthesized polyethylene glycol-dihyd-poly lactic acid (PEG-dihyd-PLA) micelles containing pH-sensitive hydrazone bonds, and the release rates of these micelles in physiological (pH 7.4) and acidic environment (pH 4.5) were 38% and 75% in 24 h, respectively.[38] Lee et al. synthesized doxorubicin-conjugated poly(ethylene oxide)-poly(propylene oxide)-poly(ethylene oxide (PEO–PPO–PEO) copolymer via a hydrazone bond, and the DOX released out of micelles was 40% and 84% in pH 5 and pH 7.4 after 26 h, respectively.[39] Furthermore, depending on release studies of nanoparticles consisting of an acetal bond in the previous studies, Chen et al. synthesized acetal base linkage containing pH-responsive biodegradable micelles, and according to their result, 98%, 89%, and 44% DOX were released at pH 4.0, 5.0, and pH 7.4 within 48 h, respectively.[40]

Also, DOX release from a pH-insensitive carrier usually exhibits low pH sensitivity (release rate at 5.0 is about 1.8 times or less than neutral pH) as stated in the Jia et al. study. In our study, we reached 2.5-fold faster release at acidic pH compared to release at pH 7.4, which can be accepted as pH-dependent drug release.[8]

It is obvious that the findings related to the DOX release from the micelle based on acetal-based cross-links and hydrazone bond are consistent with the similar studies in literature and allowed better drug release control.[8,29,30] It should also be noted that using a cross-linking strategy in micelle structure allowed a more stable system in blood circulation. As a result, we obtained a nanocarrier system which is stable in blood circulation with less disintegration in micelle assembly and dual-responsive pH sensitivity inside the cell facilitating intracellular drug release.

3.4. Degradation of Micelles

Due to acid-degradable bonds in the core cross-links of the micelles, they are expected to degrade at acidic conditions. In order to prove this, micelles (CCM2) were incubated at pH 4.5, 37 °C for 24 h. Samples were withdrawn from the medium (between 0 and 24 h) and analyzed by DLS, FTIR, and GPC. First, micelle degradation was chemically showed by FTIR (**Figure 6**A1,A2). It is evident that the intensity of the acetal group's peak around 1100 cm^{-1} decreased after acidic degradation (Figure 6A2). According to the size analysis (Figure 6B), the diameters of the particles were decreased while PDIs were increased with degradation time beginning within 2 h. It demonstrated the formation of smaller chains causing higher PDIs by degradation. This was also proved by GPC in which the retention volume of the particles shifted to larger values meaning that the size of particles was smaller and eluting from the column later (Figure S8, Supporting Information). In the literature, Bhuchar et al. and Wang et al. prepared nanogels using 2,2-dimethacroyloxy-1-ethoxypropane (DMAEP) that is the same as our cross-linker, and they observed that their nanogels were unstable in the acidic environment (pH 4.5 and pH 5.2), which resulted in degradation within 2 h by measuring the hydrodynamic diameter.[19,41] To sum up, CCMs produced in this study can be degraded into tiny particles that can facilitate the drug release by the effect of pH, which was supported with the literature.

To check the stability of the micelles for 6 months, we performed size analysis in PBS and observed that micelles

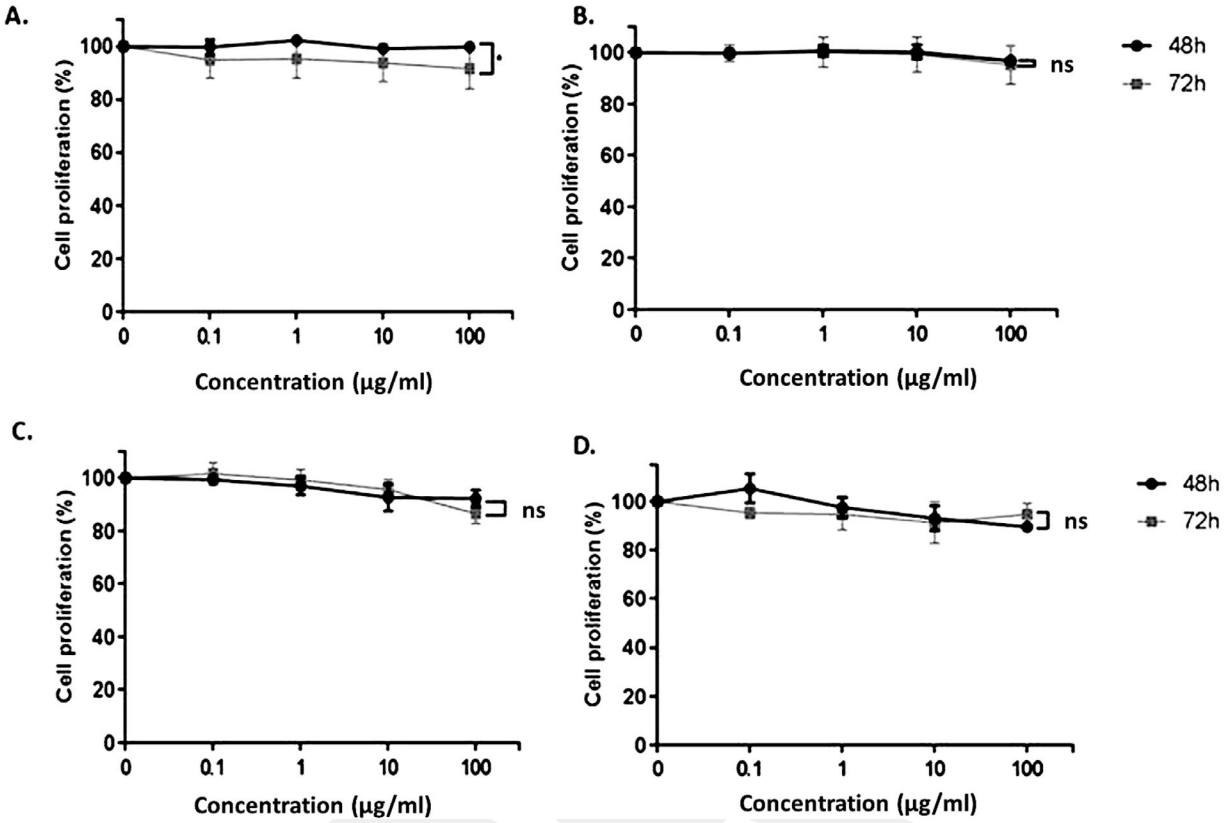

Figure 7. Cytotoxic effects of free NCs on cell proliferation of A) SKBR-3 and B) MCF-10A cells and free HER2-NCs on cell proliferation of C) SKBR-3 and D) MCF-10A cells at 48 and 72 h.

maintained their sizes at these conditions. Size and size distribution of CCMs in PBS were given as Figure S9 (Supporting Information). Also, we performed an experiment in blood-simulated solution to check stability in the blood, and no change in the micelle size was observed at 37 °C, even after 1 week (Figure S10, Supporting Information). As a result, these NCs are stable in PBS up to 6 months, which means we can keep them for weeks in these conditions. Besides, in the case of intravenous (i.v.) administration, these NCs may keep their stability in terms of size up to 1 week following the injection.

3.5. Cytotoxicity Results

The cytotoxicity of free NCs and their targeted forms (HER2-NCs) against SKBR-3 and MCF-10A was explored by XTT assay. The results showed that the cell viability of SKBR-3 and MCF-10A cells was slightly dependent on the NC amount. The viability of the cells was higher than 80% at the concentrations from 0.1 to 100 μg mL^{-1} at both 48 and 72 h of incubation (**Figure 7**).

Furthermore, the cytotoxicity of DOX-conjugated formulations (DOX-NCs and DOX-HER2-NCs) against SKBR-3 and MCF-10A cells was evaluated. Step-wise increasing concentrations of DOX (at 48- and 72 hours), DOX-NCs (at 48 hours), and DOX-HER2-NCs (at 48 hours) ((0.1–5) × 10^{-6} M) for SKBR-3 cells and DOX (at 48- and 72 hours) , DOX-NCs (at 48 hours), and DOX-HER2-NCs (at 48 hours) ((0.05–1) × 10^{-6} M) for MCF-10A cells were used to determine inhibitory concentration (IC50-half-maximal inhibitory concentration) value (**Figure 8**).

The IC_{50} values of DOX were calculated as 0.65 × 10^{-6} and 0.61 × 10^{-6} M for SKBR-3 cells at 48 and 72 h, respectively (Figure 8A). Besides, The IC_{50} values of DOX were 0.08 × 10^{-6} and 0.1 × 10^{-6} M for MCF-10A cells at 48 and 72 h, respectively (Figure 8B). These results were used to decide the concentration range of DOX-NCs and DOX-HER2-NCs in the cell proliferation assays against SKBR-3 and MCF-10-A cell lines. The results revealed that the IC_{50} values of DOX-NCs and DOX-HER2-NCs were 1.07 × 10^{-6} and 0.45 × 10^{-6} M for SKBR-3 cells at 48 h, respectively (Figure 8C). The significant change was on both DOX-NCs and DOX-HER2-NCs. According to IC_{50} values, DOX-HER2-NCs were twofold more effective on SKBR-3 cells as compared to DOX-NCs, which shows the targeting effect of the HER2-specific peptide on breast cancer cells (Figure 8C). Note that the addition of targeting peptide to NCs did not reveal any difference in terms of selectivity for MCF-10A cells, which demonstrates no preferential uptake of targeted NCs by healthy cells according to the IC_{50} values (0.15 × 10^{-6} and 0.18 × 10^{-6} M for MCF-10A cells of DOX-NCs and DOX-HER2-NCs at 48 h, respectively) (Figure 8D). In other words, DOX-NCs and DOX-HER2-NCs exhibited almost similar cytotoxic effects on MCF-10A. The effects of DOX-HER2-NCs were higher on HER2 overexpressed SKBR-3 cells. Kim et al. and Panikar et al. reported that DOX-loaded HER2-binding peptide-conjugated micelles applied on HER2-overexpressing SKBR3 breast cancer cells exhibited selectivity for

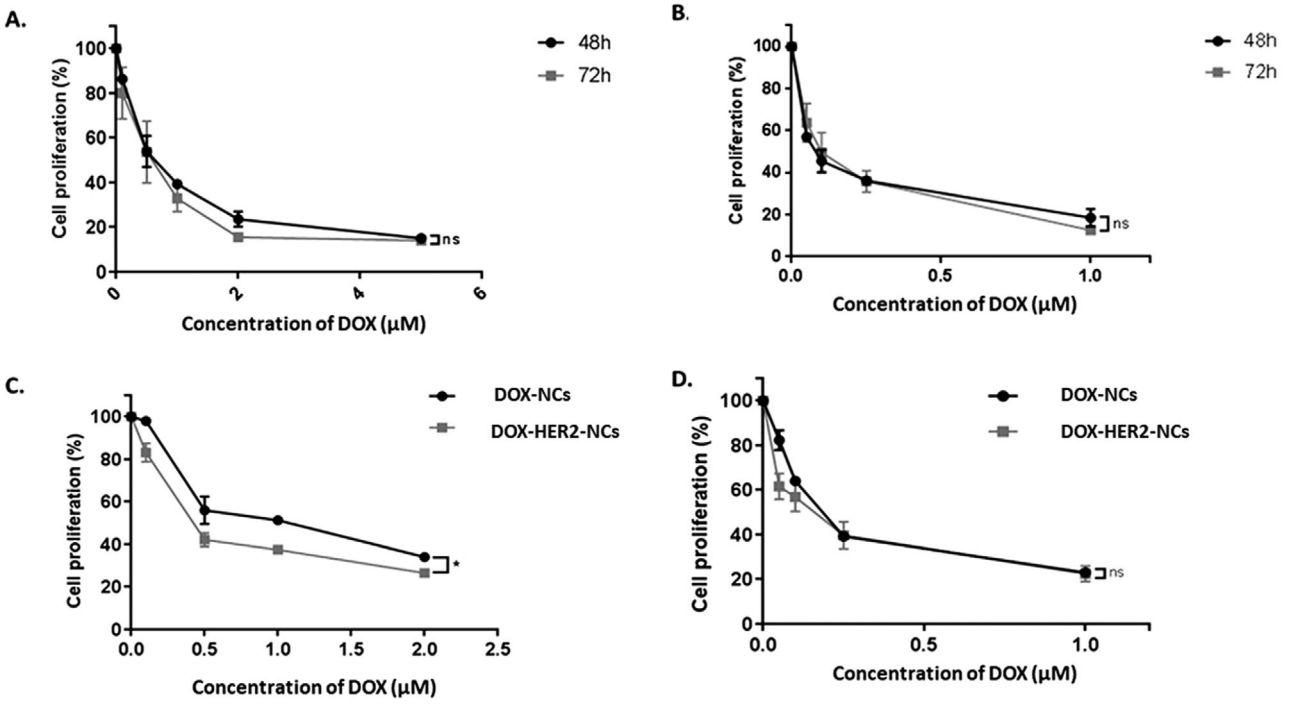

Figure 8. Cytotoxic effect of DOX on cell proliferation of A) SKBR-3 and B) MCF-10-A cells at 48 and 72 h. DOX-NCs and DOX-HER2-NCs on cell proliferation of C) SKBR-3 and D) MCF-10-A cells at 48 h.

HER2-positive breast tumor cells.[42,43] According to the study of Kim et al., efficiency of targeted nanoparticles was about more 1.2-fold than nontargeted nanoparticles.[42] Also, the IC_{50} value of 0.45×10^{-6} M for DOX-HER2-NCs against SKBR-3 cells revealed that DOX-conjugated HER2 micelles increased the effect of DOX as compared to both only DOX and DOX-NCs at 48 h application. Moreover, according to the IC_{50} values (0.08×10^{-6}, 0.15×10^{-6}, and 0.18×10^{-6} M for the naked DOX, DOX-NCs, and DOX-HER2-NCs at 48 h, respectively), we observed less toxicity toward MCF-10A cells, and it means that using NC with or without peptide revealed a kind of masking effect on the toxicity by DOX.

3.6. Intracellular Uptake of NCs

The uptake of 1.07×10^{-6} M DOX-NCs (IC_{50} concentration) and 0.45×10^{-6} M DOX-HER2-NCs (IC_{50} concentration) by SKBR-3 cells at 48 h were determined by fluorescence imaging (**Figure 9**). For this purpose, ten different images were processed by using ImageJ. The concentration of IC_{50} values of NCs for SKBR-3 cells was applied, and it was shown that the fluorescence intensity density value of DOX-NCs-HER2 is higher as compared to DOX-NCs despite a low-concentration application of DOX-NCs-HER2. The conjugated HER2 peptide on NCs provided a high uptake rate by SKBR-3 cells (Figure 9A). After unpaired statistical analysis, the fluorescence intensity density value of DOX-NCs-HER2 is fourfold more than DOX-NCs on SKBR-3 cells. This difference was also significant. This result revealed that the DOX-NCs-HER2 was more effective than DOX-NCs on SKBR-3 HER2 positive cells. High cytotoxic effects of DOX-HER2-NCs on SKBR-2 cells can be explained by more intracellular uptake of DOX molecules.

These results showed that targeted DOX-HER2-NCs increased the uptake of DOX by HER2-enriched SKBR-3 cells. The colocalization value of DOX-HER2-NCs was higher than DOX-NCs on SKBR-3 cells. This difference was determined by using unpaired *t*-test statistical analysis. Therefore, a significant change was found between the application of DOX-NCs and DOX-HER2-NCs on SKBR-3 cells (Figure 9A). The IC_{50} value of NCs was applied to MCF-10A cells, and the results showed that the fluorescence intensity density values of DOX-NCs-HER2 and DOX-NCs were similar (Figure 9B) due to the absence of HER2 receptor on MCF-10A cells.

It was shown that the efficiency of DOX-HER2-NCs was higher than DOX-NCs. Besides, the distribution of DOX is also different for DOX-HER2-NCs and DOX-NCs that was identified by the colocalization analysis of DOX (red) and DAPI (nuclei dye-blue), which can be seen from **Figure 10**. It is evident that there was no significant change in MCF-10A cells because of the absence of HER2 receptor in these cells. Besides the determination of fluorescence intensity density on SKBR-3 cells for DOX-NCs and DOX-HER2-NCs, the localization of DOX molecules was different. The localization of DOX molecules was determined by using FIJI imaging processes program. For this purpose, the colocalization analysis was used with localization of DAPI and DOX. The images of DAPI and DOX at different wavelengths were merged and *R*-total value was calculated by three images. The *R*-total value represents the colocalization value. If it is closed to "1," two different images from different fluorescence wavelengths are colocalized, which is determined by the Pearson's correlation coefficient.

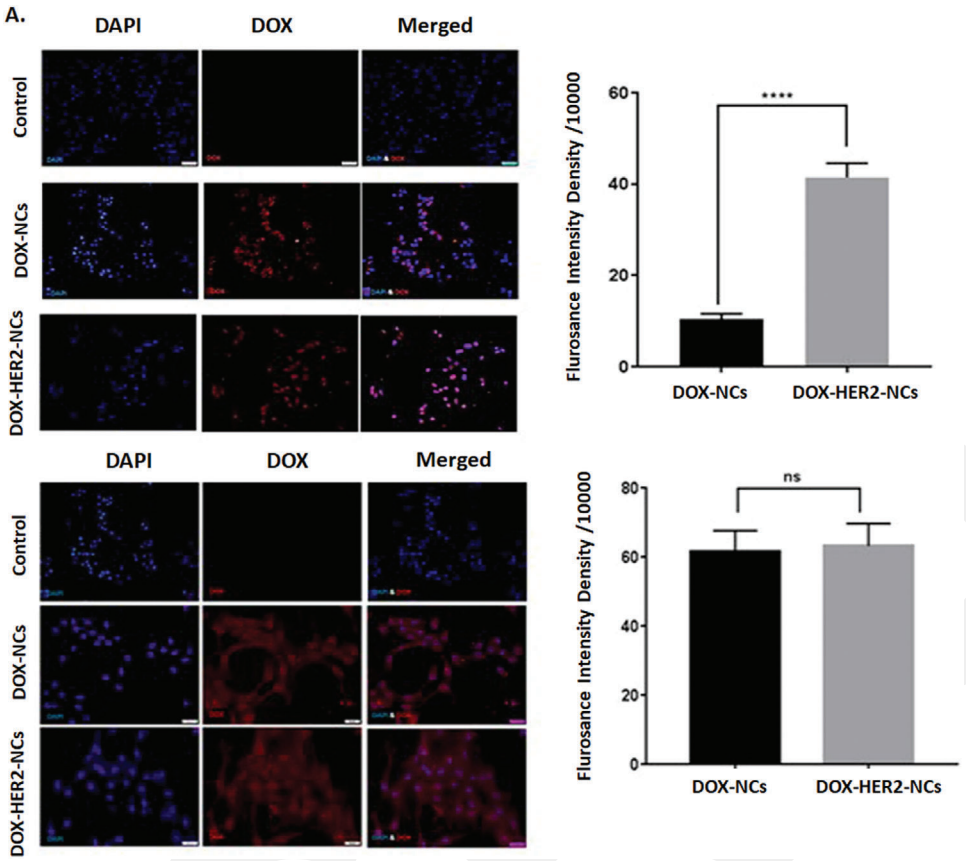

Figure 9. Fluorescence images and fluorescence intensity density of DOX-NCs and DOX-HER2-NCs for A) SKBR-3 and B) MCF-10A cells at 48 h. Magnification: 20×, blue: DAPI; red: DOX.

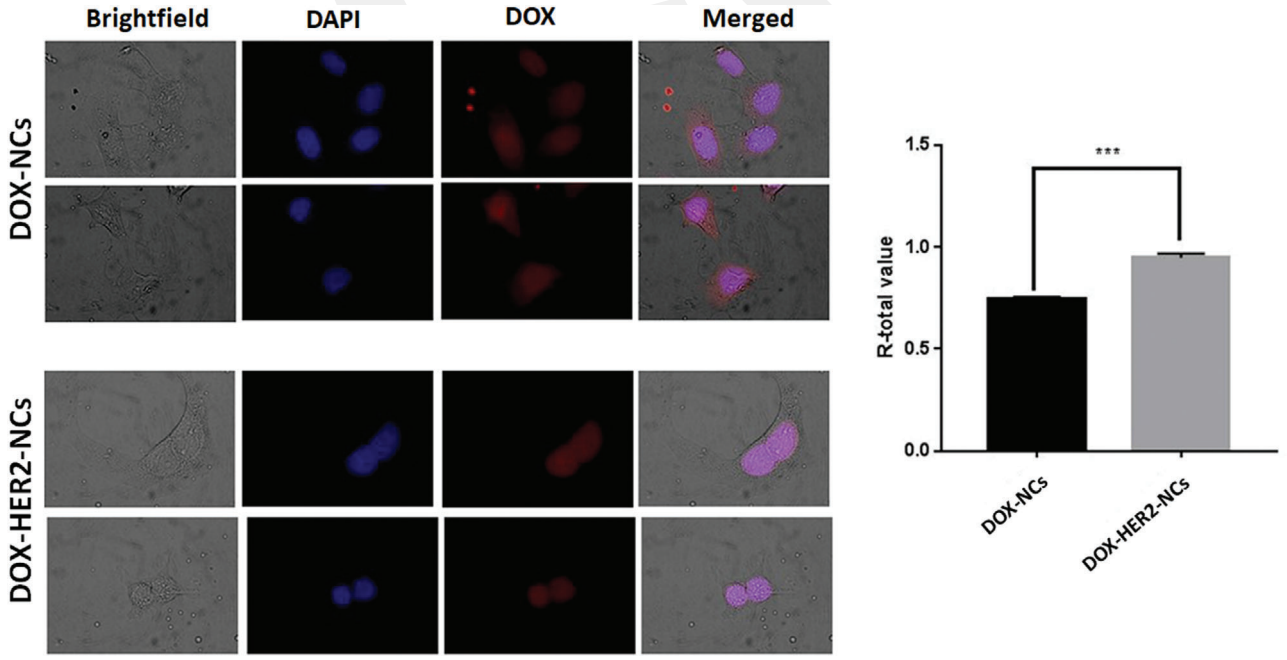

Figure 10. *R*-total value (co-localization) of DOX-NCs and DOX-HER2-NCs for SKBR-3 cells at 48 h, Magnification: 100×; blue: DAPI; red: DOX.

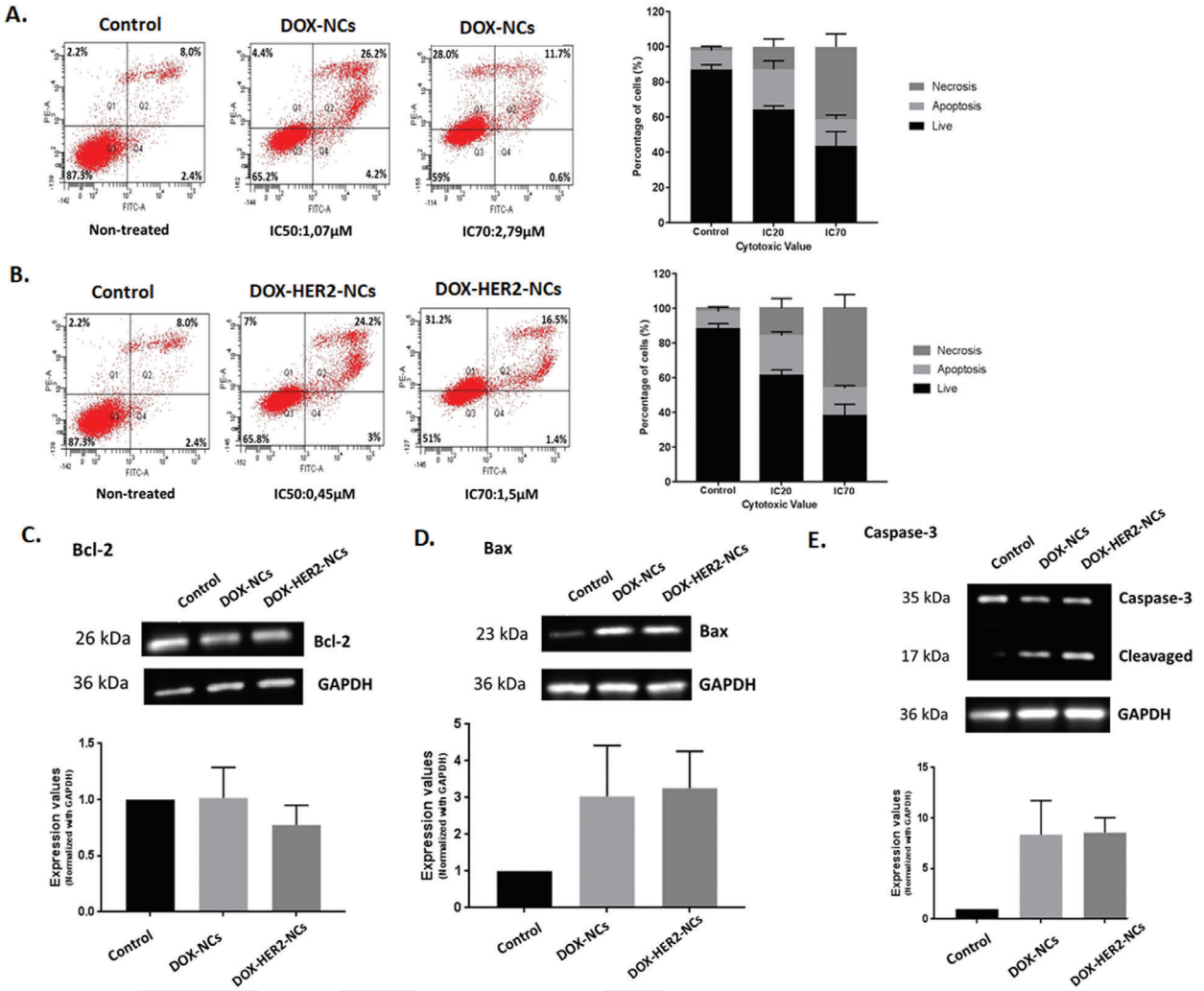

Figure 11. The apoptotic effects of A) DOX-NCs and B) DOX-HER2-NCs on SKBR-3 cells, and on C) Bcl-2, D) Bax, and E) Caspase-3 protein expression levels at 48 h.

The localization of drug in cells is important to understand the targeting mechanism of drug. This difference can be occurred because of application dose of NCs and drug release mechanism. According to the images, the mechanism of action for targeted and nontargeted NCs was different on SKBR-3 cells owing to the localization of DOX-NCs and DOX-HER2-NCs. This event can be occurred with two possibilities. The first reason is the drug concentration because of the different application doses caused by the IC_{50} values of DOX-NCs and DOX-HER2-NCs. The other reason is the effect of the drug mechanism on SKBR-3 cells, in which the targeted property of DOX-HER2-NCs induces tracking of nucleus in SKBR-3 cells. However, it did not occur after the application of DOX-NCs, which reveals the localization of DOX-NCs in cytoplasm.

These results are also consistent with the study of Chen et al. in which DOX-loaded pH-responsive polymeric micelles conjugated with HER2 peptide exhibited a better accumulation in tumor cell uptake compared to the nontargeted micelles.[44] As shown in our study with the fluorescence intensity density method, tumor-specific peptide-conjugated nanoparticles induce cellular uptake of DOX, which is supported by the intracellular accumulation in tumor cells.

Because this is a nanoparticle system, we should also make assessment of the size and zeta potential of nanoparticles and their possible contribution to the cellular uptake. According to the Zhang et al. study, nanoparticle internalization by tumor cells was increased when the zeta potential value changes from negative to positive values.[45] In our study, the zeta potentials of DOX-NCs and DOX-HER2-NCs (in water) are -18.23 ± 0.51 and -16.90 ± 0.36, respectively. These values are -6.24 ± 0.47 and -6.45 ± 0.34, respectively for DOX-NCs and DOX-HER2-NCs in PBS. In both cases, the zeta potential differences between targeted and nontargeted micelles are not very high. Due to this fact, the zeta potential value cannot be determinant for the selective internalization in this study. The presence of a targeting ligand is more effective for this selectivity toward HER(+) cells, as expected.

It is a well-known phenomenon that small-sized nanoparticles were uptaken by the cell more effectively.[46] As we have already given before, the sizes of DOX-NCs and DOX-HER2-NCs were 99

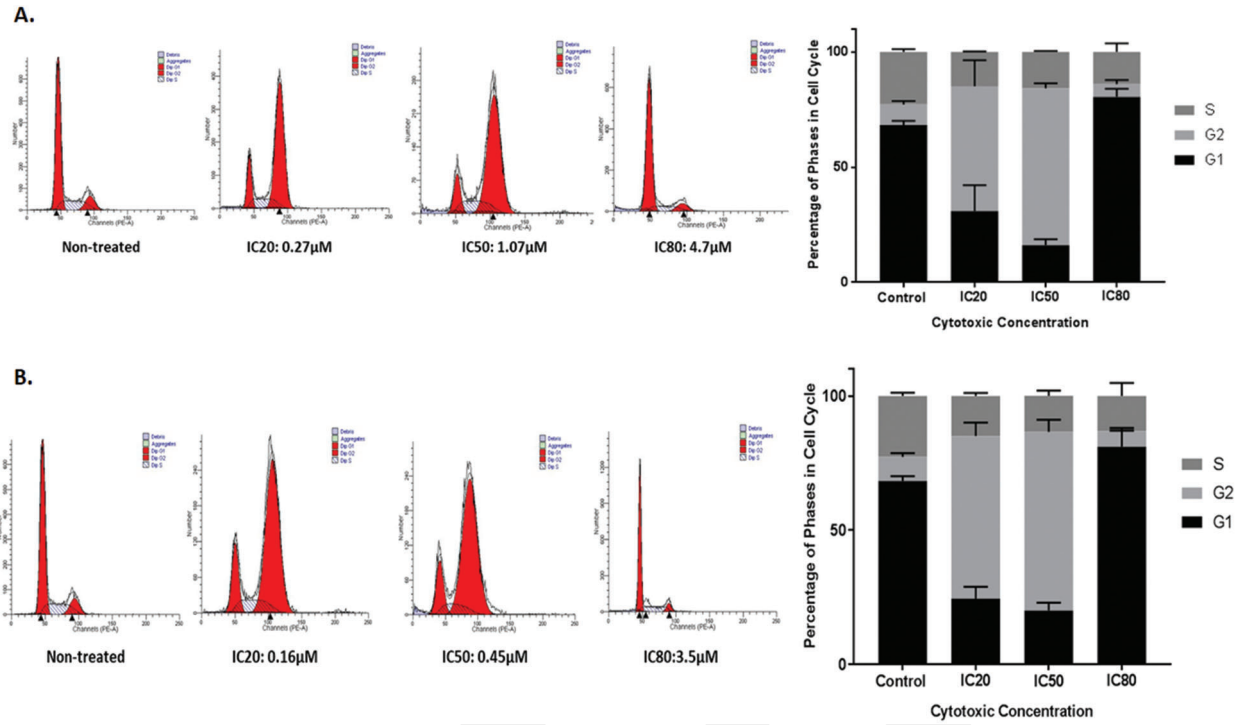

Figure 12. Effects of A) DOX-NCs and B) DOX-HER2-NCs on cell cycle phases of SKBR-3 at 48 h.

and 116 nm, respectively (Figure S7, Supporting Information). The effect of using a targeting peptide for the specific uptake here is most probably higher than the effect of NCs' sizes because there is a quite small difference (17 nm). Note that we have not observed any difference between the uptake of DOX-NCs and DOX-HER2-NCs by MCF-10A cells, which demonstrates the importance of a ligand presence even if these particles have different sizes or charges. According to the cell proliferation and imaging data given above, targeted ones are preferentially uptaken by SKBR-3 cells due to the presence of HER2 receptor. Therefore, we can conclude that the receptor–ligand interaction for cell uptake has more important contribution on cell uptake than particles' zeta potential and size in a targeted NC case.

3.7. Apoptotic Effects of NCs on Cells

IC_{50} and IC_{70} values of DOX-NCs and DOX-HER2-NCs were applied on SKBR-3 cells at 48 h to define apoptosis and necrosis percentages by Annexin V/PI double staining assay. Besides, the expression levels of pro-apoptotic and anti-apoptotic proteins were determined by western Blotting.

Increasing the doses of DOX-NCs and DOX-HER2-NCs increased the percent of apoptotic cell population as well as induced necrosis (**Figure 11**A,B). The low doses of DOX-HER2-NCs are more effective than DOX-NCs on SKBR-3 cells.

Bcl-2 protein is involved in the regulation of apoptotic cell death. In this experiment, GAPDH was used as internal positive control to understand the changes in protein levels of Bcl-2. The results showed that there was a small decrease in protein levels of Bcl-2 in response to DOX-HER2-NCs' application (Figure 11C). During this experiment, 1.07×10^{-6} M of DOX-NCs and 0.45×10^{-6} M of DOX-HER2-NCs were used to determine Bcl-2 protein level. In this step, the IC_{50} value was trailed because the apoptosis was observed in Annexin V/PI double staining while increasing doses of DOX-NC- and DOX-HER2-NC-induced necrosis.

In parallel with determining the protein levels of pro-apoptotic Bax protein, we analyzed protein levels of GAPDH, which is used as internal positive control. The results showed that the protein levels of Bax were increased in response to DOX-NCs and DOX-HER2-NCs as compared to control (Figure 11D). During this experiment, 1.07×10^{-6} M of DOX-NCs and 0.45×10^{-6} M of DOX-HER2-NCs were used to determine protein levels of Bax. Application of DOX-NCs and DOX-HER2-NCs increased protein levels of pro-apoptotic Bax in which low dose of DOX-HER2-NCs and high dose of DOX-NCs had the similar effect. Therefore, low dose of DOX-HER2-NCs was more effective than high dose of DOX-NCs. The mechanism of action for DOX-HER2-NCs was related to Bax protein. Low dose of DOX-HER2-NCs induce Bax protein without Bcl-2 protein.

Apoptotic pathways are orchestrated by caspases, a family of cysteine proteases, and cleavage on the carboxy-terminal side of specific aspartic acid residues. Caspase-3 protein is a member of Caspase family. The cleavage of Caspase-3 provides fragment formation that is detected with substrate-specific antibodies. The results revealed that Caspase-3 was cleaved and observed as 17 and 35 kDa in response to IC_{50} doses of DOX-NCs and DOX-HER2-NCs at 48 h. The rate of cleavage of Caspase-3 was increased as compared to noncleaved control. This result showed that treatment of DOX-NCs and DOX-HER2-NCs at 48

h induce apoptosis. In addition, the DOX-HER2-NCs is more effective than DOX-NCs on SKBR-3 cells since low dose of DOX-HER2-NCs and high dose of DOX-NCs had similar effects. The IC_{50} doses of DOX-NCs and DOX-HER2-NCs were 1.07×10^{-6} and 0.45×10^{-6} M, respectively (Figure 11E).

Furthermore, targeted nanoparticles strongly inhibit and decrease cell proliferation through triggered apoptosis. It can be concluded that the targeted nanoparticles induce apoptotic pathway, resulting in an activation of apoptotic proteins such as Bax and Caspase-3 or reduction of anti-apoptotic proteins such as Bcl-2.[47,48] Shen et al. demonstrated a similar role of copolymeric pH-responsive nanoparticles on SKBR-3 cell, in which pH-responsive and targeted nanoparticles inhibited the cell viability and decreased the apoptosis rate of SKBR-3 cells by using Annexin V–PI apoptosis.[49]

3.8. Cytostatic Effects of NCs on Cells

SKBR-3 cells treated with 0.27×10^{-6} and 1.07×10^{-6} M of DOX-NCs increased G2 phase and decreased G1 phase of the cell cycle. However, applications of 4.7×10^{-6} M of DOX-NCs on SKBR-3 cells increased G1 phases of cell cycle (**Figure 12**A). SKBR-3 cells treated with 0.16×10^{-6} and 0.45×10^{-6} M of DOX-HER2-NCs increased G2 phase and decreased G1 phase in the cell cycle. However, there were no significant differences between 0.16×10^{-6} and 0.45×10^{-6} M. The applications of 3.5×10^{-6} M of DOX-HER2-NCs on SKBR-3 cells increased G1 phase of the cell cycle (Figure 12B). The effects of DOX-NCs and DOX-HER2-NCs on cell cycle progression of SKBR-3 were similar. Since it is known that DOX has cytotoxic effects, is an inhibitor of topoisomerases II that cause G1 and G2 cell cycle arrest and the increase of apoptosis, it was predicted that the DOX-attached NCs would affect the cell cycle.[50,51] The important point is that although lower doses of DOX-HER2-NCs were applied as compared to DOX-NCs in the study, DOX-HER2-NCs were more specific and selective for SKBR-3 cells than DOX-NCs.

4. Conclusion

In this study, we prepared breast-cancer-targeted, core cross-linked polymeric micelle with double-moiety pH sensitivity, in which the drug is conjugated to the polymer with pH-degradable hydrazone bonds, and the micelle is core cross-linked with pH-degradable acetal bonds. All physicochemical analyses showed that uniform micelle NCs were produced thanks to RAFT polymerization for the controlled and one-step synthesis of CCMs. We obtained stable micellar NCs at physiological pH and achieved acid-triggered drug release by the synergistic effect of both acetal-based cross-links of the micelle core and hydrazone bond. We achieved 31% pH-triggered drug release in this study with our nanocarrier. Even though we used chemical conjugation here, we thought that physically bound DOX is also present here due to the chemical nature of the micellar components in the core. We think that the micellar structure should be designed to achieve a fewer physical interactions with drug. Also, the purification methods should be specific to the designed nanocarrier system by taking additional cautions.

The efficacy of the proposed system was demonstrated by cell viability experiments. The cytotoxicity of the "smart" NCs was investigated toward SKBR3 cells with control of MCF-10A.

Furthermore, HER2 peptide (VSSTQDFP) and DOX-conjugated micelles' apoptotic and cytostatic effects were evaluated on breast cancer cells. The results of cell proliferation and viability assays revealed that DOX-HER2-NCs are more effective on SKBR-3 cells at 48 h because of HER2 receptor on these cells. Moreover, the fluorescence intensity density in SKBR-3 cells was higher when these cells were treated with DOX-HER2-NCs compared to DOX-NCs. DOX-HER2-NCs and DOX-NCs had the same effects on MCF-10A cells in terms of fluorescence intensity density. In addition to that, the DOX-HER2-NCs were localized in the nucleus of SKBR-3 cells, while DOX-NCs were scattered in the cytoplasm. These results confirmed the selective targeting by HER2-specific peptide carrying NCs toward SKBR-3 cells. Also, the application of DOX-NCs and DOX-HER2-NCs induced apoptosis and primary necrosis by specific apoptotic proteins. Also, these NCs induce cell cycle arrest.

In conclusion, produced HER2-targeted acid-degradable core cross-linked micelles selectively affect the tumor cells. All the detailed in vitro studies show that these micelles have great potential as an efficient alternative to the conventional treatment methods against HER2 positive breast cancer.

Supporting Information

Supporting Information is available from the Wiley Online Library or from the author.

Acknowledgements

N.N.B. and G.T.U. contributed equally to this work. This work was supported by the Scientific and Technological Research Council of Turkey (TÜBİTAK), Project Number: 116R057. N.N.B. and G.T.U. were supported by TÜBİTAK 116R057. The authors also thank Hacettepe University, Advanced Technologies Research and Application Center (HUNİTEK) for MALDI-TOF MS analysis.

Conflict of Interest

The authors declare no conflict of interest.

Data Availability Statement

The data that support the findings of this study are available from the corresponding author upon reasonable request.

Keywords

breast cancer, cross-linked micelles, dual pH-responsiveness, HER2 targeting, micelle nanocarriers, RAFT polymerization

Received: September 19, 2021
Revised: October 20, 2021
Published online: November 9, 2021

[1] E. Pérez-Herrero, A. Fernández-Medarde, *Eur. J. Pharm. Biopharm.* **2015**, *93*, 52.
[2] Y. Shi, R. van der Meel, X. Chen, T. Lammers, *Theranostics* **2020**, *10*, 7921.
[3] I. A. Isoglu, Y. Ozsoy, S. D. Isoglu, *Curr. Top. Med. Chem.* **2017**, *17*, 1469.
[4] M. Talelli, M. Barz, C. J. F. Rijcken, F. Kiessling, W. E. Hennink, T. Lammers, *Nano Today* **2015**, *10*, 93.
[5] I. Biancacci, Q. Sun, D. Möckel, F. Gremse, S. Rosenhain, F. Kiessling, M. Bartneck, Q. Hu, M. Thewissen, G. Storm, W. E. Hennink, Y. Shi, C. J. F. Rijcken, T. Lammers, A. M. Sofias, *J. Controlled Release* **2020**, *328*, 805.
[6] B. J. Crielaard, C. J. Rijcken, L. Quan, S. van der Wal, I. Altintas, M. van der Pot, J. A. Kruijtzer, R. M. Liskamp, R. M. Schiffelers, C. F. van Nostrum, W. E. Hennink, D. Wang, T. Lammers, G. Storm, *Angew. Chem., Int. Ed.* **2012**, *51*, 7254.
[7] X. T. Cao, C. M. Le, H. Thi, G.-D. Kim, Y. Gal, K. Lim, *eXPRESS Polym. Lett.* **2017**, *11*, 832.
[8] Z. Jia, L. Wong, T. P. Davis, V. Bulmus, *Biomacromolecules* **2008**, *9*, 3106.
[9] L. Zhang, J. Bernard, T. P. Davis, C. Barner-Kowollik, M. H. Stenzel, *Macromol. Rapid Commun.* **2008**, *29*, 123.
[10] T. Ramasamy, H. B. Ruttala, B. Gupta, B. K. Poudel, H. G. Choi, C. S. Yong, J. O. Kim, *J. Controlled Release* **2017**, *258*, 226.
[11] S. Binauld, M. H. Stenzel, *Chem. Commun.* **2013**, *49*, 2082.
[12] H. Wei, R.-X. Zhuo, X.-Z. Zhang, *Prog. Polym. Sci.* **2013**, *38*, 503.
[13] A. D. Friedman, S. E. Claypool, R. Liu, *Curr. Pharm. Des.* **2013**, *19*, 6315.
[14] G. T. Hermanson, in *Bioconjugate Techniques*, 2nd ed. (Ed: G. T. Hermanson), Academic Press, New York, NY **2008**, p. 1.
[15] F. Masood, *Mater. Sci. Eng., C* **2016**, *60*, 569.
[16] G. Abbineni, S. Modali, B. Safiejko-Mroczka, V. A. Petrenko, C. Mao, *Mol. Pharmaceutics* **2010**, *7*, 1629.
[17] N. Gandra, G. Abbineni, X. Qu, Y. Huai, L. Wang, C. Mao, *Small* **2013**, *9*, 215.
[18] M. Topuzoğullari, V. Bulmus, E. Dalgakiran, S. Dincer, *Polymer* **2014**, *55*, 525.
[19] N. Bhuchar, R. Sunasee, K. Ishihara, T. Thundat, R. Narain, *Bioconjugate Chem.* **2012**, *23*, 75.
[20] C. Boyer, A. Granville, T. P. Davis, V. Bulmus, *J. Polym. Sci., Part A: Polym. Chem.* **2009**, *47*, 3773.
[21] V. Bulmus, Y. Chan, Q. Nguyen, H. L. Tran, *Macromol. Biosci.* **2007**, *7*, 446.
[22] C. Boyer, V. Bulmus, T. P. Davis, *Macromol. Rapid Commun.* **2009**, *30*, 493.
[23] M. B. Thomas, K. Radhakrishnan, D. P. Gnanadhas, D. Chakravortty, A. M. Raichur, *Int. J. Nanomed.* **2013**, *8*, 267.
[24] Y. Zhou, Z. Guo, Y. Zhang, W. Huang, Y. Zhou, D. Yan, *Macromol. Biosci.* **2009**, *9*, 1090.
[25] D. J. Keddie, *Chem. Soc. Rev.* **2014**, *43*, 496.
[26] M. R. Shah, M. Imran, S. Ullah, in *Nanocarriers for Cancer Diagnosis and Targeted Chemotherapy* (Eds: M. R. Shah, M. Imran, S. Ullah), Elsevier, Amsterdam, The Netherlands **2019**, p. 1.
[27] D. Willner, P. A. Trail, S. J. Hofstead, H. D. King, S. J. Lasch, G. R. Braslawsky, R. S. Greenfield, T. Kaneko, R. A. Firestone, *Bioconjugate Chem.* **1993**, *4*, 521.
[28] F. Kratz, U. Beyer, P. Collery, F. Lechenault, A. Cazabat, P. Schumacher, U. Falken, C. Unger, *Biol. Pharm. Bull.* **1998**, *21*, 56.
[29] M. Hrubý, Č. Koňák, K. Ulbrich, *J. Controlled Release* **2005**, *103*, 137.
[30] A. Mahmud, X.-B. Xiong, A. Lavasanifar, *Eur. J. Pharm. Biopharm.* **2008**, *69*, 923.
[31] F.-Q. Hu, L.-N. Liu, Y.-Z. Du, H. Yuan, *Biomaterials* **2009**, *30*, 6955.
[32] H. S. Yoo, T. G. Park, *J. Controlled Release* **2001**, *70*, 63.
[33] H. H. Chen, W. C. Huang, W. H. Chiang, T. I. Liu, M. Y. Shen, Y. H. Hsu, S. C. Lin, H. C. Chiu, *Int. J. Nanomed.* **2015**, *10*, 5035.
[34] A. Suo, J. Qian, Y. Yao, W. Zhang, *Int. J. Nanomed.* **2010**, *5*, 1029.
[35] L. Wong, M. Kavallaris, V. Bulmus, *Polym. Chem.* **2011**, *2*, 385.
[36] X. Wang, G. Wu, C. Lu, W. Zhao, Y. Wang, Y. Fan, H. Gao, J. Ma, *Eur. J. Pharm. Sci.* **2012**, *47*, 256.
[37] K. Kataoka, T. Matsumoto, M. Yokoyama, T. Okano, Y. Sakurai, S. Fukushima, K. Okamoto, G. S. Kwon, *J. Controlled Release* **2000**, *64*, 143.
[38] P. Qi, X. Wu, L. Liu, H. Yu, S. Song, *Front. Pharmacol.* **2018**, *9*, 12.
[39] Y. Lee, S. Y. Park, H. Mok, T. G. Park, *Bioconjugate Chem.* **2008**, *19*, 525.
[40] W. Chen, F. Meng, F. Li, S. J. Ji, Z. Zhong, *Biomacromolecules* **2009**, *10*, 1727.
[41] Y. Wang, J. Zheng, Y. Tian, W. Yang, *J. Mater. Chem. B* **2015**, *3*, 5824.
[42] B. Kim, J. Shin, J. Wu, D. T. Omstead, T. Kiziltepe, L. E. Littlepage, B. Bilgicer, *J. Controlled Release* **2020**, *322*, 530.
[43] S. S. Panikar, G. Ramírez-García, A. A. Vallejo-Cardona, N. Banu, O. A. Patrón-Soberano, D. Cialla-May, T. A. Camacho-Villegas, E. de la Rosa, *Nanoscale* **2019**, *11*, 20598.
[44] Q. Chen, M. Long, L. Qiu, M. Zhu, Z. Li, M. Qiao, H. Hu, X. Zhao, D. Chen, *Int. J. Nanomed.* **2016**, *11*, 5415.
[45] Y. Zhang, M. Yang, N. G. Portney, D. Cui, G. Budak, E. Ozbay, M. Ozkan, C. S. Ozkan, *Biomed. Microdevices* **2008**, *10*, 321.
[46] M. Saadat, F. Zahednezhad, P. Zakeri-Milani, H. Reza Heidari, J. Shahbazi-Mojarrad, H. Valizadeh, *J. Pharm. Pharm. Sci.* **2019**, *22*, 191.
[47] B. Spänkuch, I. Steinhauser, H. Wartlick, E. Kurunci-Csacsko, K. I. Strebhardt, K. Langer, *Neoplasia* **2008**, *10*, 223.
[48] L. Zhang, D. Jing, N. Jiang, T. Rojalin, C. M. Baehr, D. Zhang, W. Xiao, Y. Wu, Z. Cong, J. J. Li, Y. Li, L. Wang, K. S. Lam, *Nat. Nanotechnol.* **2020**, *15*, 145.
[49] Y. Shen, J. Zhang, W. Hao, T. Wang, J. Liu, Y. Xie, S. Xu, H. Liu, *Int. J. Nanomed.* **2018**, *13*, 537.
[50] C. E. Humber, J. F. Tierney, R. P. Symonds, M. Collingwood, J. Kirwan, C. Williams, J. A. Green, *Anal. Oncol.* **2007**, *18*, 409.
[51] X. Wang, Z. Chen, A. K. Mishra, A. Silva, W. Ren, Z. Pan, J. H. Wang, *Haematologica* **2018**, *103*, 466.